

A low profile and wideband antenna with omnidirectional radiation for the sub-terahertz applications of 6G

MD. MUSHFIQUR RAHMAN^{1,*}, SUJIT HALDER^{2,*}, MD. ZULFIKER MAHMUD², TOUHIDUL ALAM^{3,4}, MOHAMMAD TARIQUL ISLAM⁵, LINI LEE¹, ABDULLAH AL MAMUN⁶, MD. SHABIUL ISLAM^{1,*}

¹Centre for Advanced Devices and Systems, Faculty of Artificial Intelligence and Engineering, Multimedia University, Persiaran Multimedia, 63100 Cyberjaya, Selangor, Malaysia.

²Department of CSE, Jagannath University, Dhaka 1100, Bangladesh

³Pusat Sains Angkasa, Institut Perubahan Iklim, Universiti Kebangsaan Malaysia, Selangor, Malaysia.

⁴Dept. Of CSE, International Islamic University Chittagong, Kumira 4318, Bangladesh

⁵Department of Electrical, Electronic and Systems Engineering, Faculty of Engineering and Built Environment, Universiti Kebangsaan Malaysia, Selangor, Malaysia.

⁶Department of Physics, University of Chittagong, Chattogram 4331, Bangladesh

This paper proposes a low-profile two-element array antenna loaded with a matching circuit to achieve miniaturized wideband characteristics with omnidirectional radiation property for the Sub Terahertz applications of 6G. A single-element antenna gives a single resonance to a low-frequency region. When the array is formed, it exhibits two resonances in the low-frequency region with poor impedance matching. However, the loading of the matching circuit improves the matching of the first resonance and aids in generating a large bandwidth for the second resonance, where the gain is also improved substantially. The inset and matching structures are optimized to get the best antenna performance. The overall compact dimension of the antenna is $600 \mu\text{m} \times 650 \mu\text{m} \times 10 \mu\text{m}$ where the height is only 0.0034 of the operating wavelengths, and the width is only one-fifth of the operating wavelength at the center frequency of the low-frequency band. The numerical simulations are done with CST microwave studio software in the time domain. Simulation results show that the compact structure gives a percentage bandwidth of 17.13 % for the first resonance ranging from 92.3 GHz to 109.6 GHz and of 82.13 % for the second resonance ranging from 147.1 GHz to 352.1 GHz where $|S_{11}|$ is less than -10 dB. Furthermore, the antenna shows a dumbbell-shaped radiation pattern in the E-plane and an omnidirectional radiation pattern in the H-plane for both resonances. Moreover, the cross-polarization levels in the H-plane for both resonances are recorded very low.

(Received September 19, 2024; accepted April 15, 2025)

Keywords: Sub-terahertz applications, 6G technology, Compact, Low-profile, Wideband, Matching circuit, Omnidirectional radiation pattern

1. Introduction

The demand for wireless connectivity has increased over the past decades, leading to developing and deploying advanced communications technologies such as 5G. Now, attention is turning to the next step in wireless communications, namely 6G, which is expected to integrate artificial intelligence, augmented reality, automation, and robotics. In addition, 6G aims to revolutionize connectivity with ultra-low latency and high data speeds. For this reason, it needs to work with very high-frequency regions, such as the Terahertz region. Several bands are newly defined in this region for the 6G technology, namely the W band (92 GHz – 114.5 GHz), D band (110 GHz – 170 GHz), G band (140 GHz – 220 GHz), and H band (220 GHz – 330GHz) [1][2]. These bands are complementary in achieving new milestones of 6G. These milestones include high capacity and wideband applications where the device with a compact low-profile antenna gives cost-effective solutions. In

addition, wideband antennae can cover narrow bands, facilitating systems with less complexity, cost, and device size, reducing the number of antennas required for a portable device. Moreover, these antennae consume less power than narrowband antennae, causing low interference. These antennae are very demandable for these benefits in applications like precision localization, medical imaging, ground penetrating radar, indoor multimedia communications, and sensor networks [3-6]. For this purpose, a compact, low-profile, and wideband antenna design becomes a competitive matter for this technology, which will play a key role in enabling seamless and cost-efficient wireless communications. Several literatures have proposed to design these types of antennas for sub-terahertz applications. In one research work [7], the patch is formed by connecting multiple branches of rectangular blocks with different lengths and widths where the branches are cut by multiple semicircular slots, and some defects are also made on the ground plane. This combination causes multiple resonances at different frequency locations with a good

level of miniaturization, but the bandwidths of all the bands are very low. On the other hand, the antenna structure proposed in [8] uses a graphene metal-based hybrid structure where a U-shaped Graphene metamaterial unit cell is inserted into a U-shaped slot, which is cut in one of the non-radiating edges of a rectangular copper patch to get low-frequency resonance. The antenna bandwidth is improved by placing two U-shaped Graphene metamaterial unit cells near the feed line. The fractional bandwidth achieved here is almost 45%, but the level of miniaturization is very poor. Moreover, a graphene-based octagonal-shaped structure is also proposed by some researchers [9] in a three-element series array to get very wideband characteristics. But the compactness achieved is not good. In another research [10], a basic rectangular patch is fed by an asymmetric coplanar waveguide port where curved slits are cut on the rectangular patch to get wideband nature. But the antenna covers a large area. Another rectangular slotted patch [11] is proposed by Abdullah Saleh Alqahtani, where miniaturization is achieved by cutting the slot in the rectangular patch. Still, the degree of compactness is not that good enough. It also shows multiband property but with narrowband characteristics. Other shapes rather than the rectangular shape are also proposed. Sina Kiani et al. researched a circular-shaped patch where they cut a slot in the patch to make a ring, and then the outer surface and the inner surface were loaded with structures like coronavirus [12]. This modification gives a very high bandwidth with a compact structure. Multilayer design is also investigated for designing wideband antennas in the sub-terahertz region. Md Hedayatullah Maktoomi et al. proposed an aperture-coupled stacked-patch antenna where a two-section distributed network is applied to get wideband property [13]. But the antenna size is very large. Patches with different shapes are also considered for terahertz applications. Murali Krishna Ch et al. proposed a modified E-shaped patch with a defected ground structure. The wideband property is achieved when a rectangular slot is cut below the transmission line [14]. This structure also shows good miniaturization property. However, further investigation is expected in this area to design compact, low-profile, and wideband antennas since the literature mentioned above has limitations in achieving either bandwidth or compactness. In addition, the wideband and compactness achieved in these research works are insufficient to fulfil the requirements of 6G. This paper investigates a two-element array of rectangular patches, each loaded with a pair of rectangular blocks and inset structures. The single rectangular patch causes resonance in the high-frequency region with poor bandwidth and gain. When the array structure is used, a dual-band characteristic with low-frequency resonance is observed with enhanced gain, but the bandwidth is still narrow, and the matching is poor. Then, a matching circuit in the form of a rectangular-shaped metallic strip is added to the middle of the array feeding network. This modification brings a tremendous change in the bandwidth. It offers a very high bandwidth. The length and width of the matching network, together with the dimensions of the inset structure and the position

of the rectangular blocks, are optimized to cause dual band characteristics with optimum wideband and miniaturized properties. The first band covers the W band, the second band covers the H band, and a portion of the G band. Good omnidirectional radiation property is also observed.

2. Antenna design and analysis

The antenna is designed on Rogers RT Duroid 5880 substrate with a thickness of 10 μm , a dielectric constant of 2.2, and a loss tangent of 0.0009. The configuration of the proposed antenna is depicted in Fig. 1, and the corresponding dimensions are listed in Table 1. Before designing this array antenna, the single antenna is designed and tested, as shown in Fig. 2 (a, b). The single antenna (Antenna 1) consists of a rectangular-shaped patch with two rectangular blocks and two inset structures connected at both sides of the patch. The inset structures are added to get better impedance matching, as shown in Fig. 3.

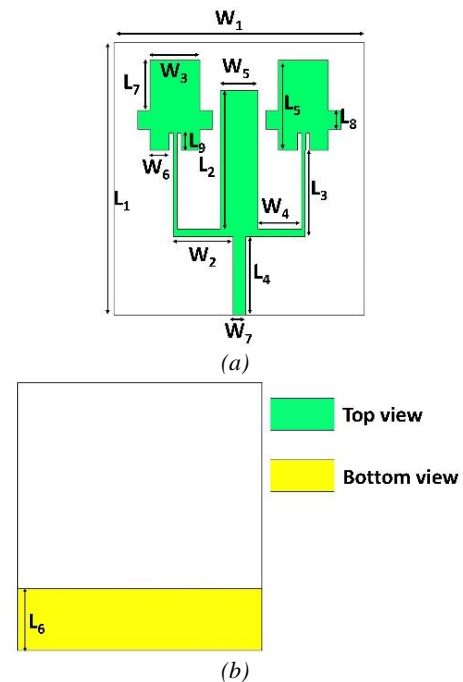


Fig. 1. The configuration of the final optimized antenna. (a) Top view. (b) Bottom view (colour online)

Table 1. Detailed dimensions of the final proposed antenna

Parameters	Values (μm)	Parameters	Values (μm)
L_1	650	W_1	600
L_2	330	W_2	142.75
L_3	205.5	W_3	120
L_4	187.5	W_4	104.25
L_5	215	W_5	90
L_6	150	W_6	45.5
L_7	120	W_7	31
L_8	45	L_9	40

This structure resonates at 194.9 GHz with an impedance bandwidth of 62 GHz ranging from 166 GHz to 228.17 GHz. The bandwidth partially covers the G band of Sub terahertz applications, which is insufficient for 6G applications. Also, the gain found in this bandwidth is poor. So, further steps are taken to improve the antenna's bandwidth and gain. It is well known that the gain improves considerably if the array structure is used. Here, a two-element array is used so that the size does not become too large, and at the same time, an enhanced gain is achieved.

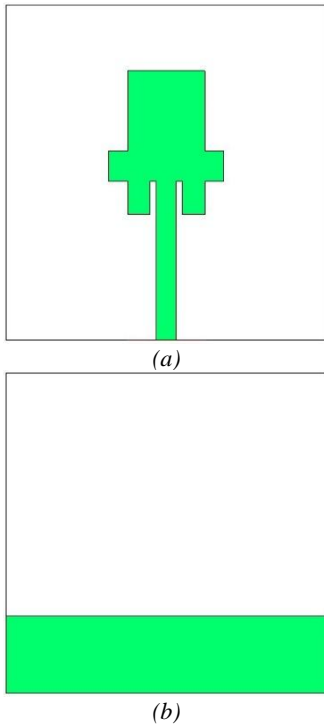


Fig. 2. (a) Patch and (b) Ground of the Antenna 1 (colour online)

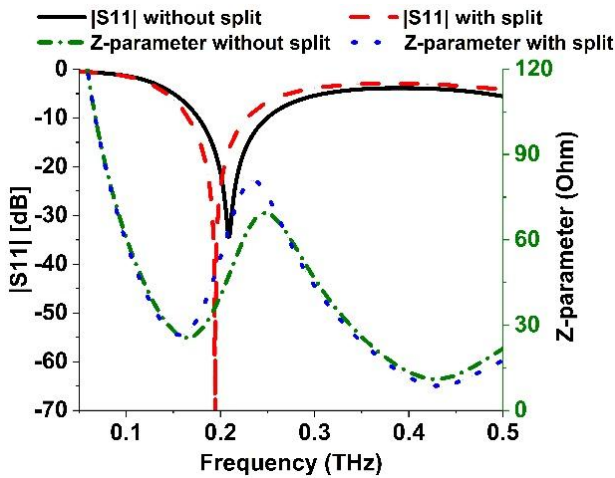


Fig. 3. Comparison of the reflection coefficients of antenna 1 with and without inset structures (colour online)

2.1. Design of array antenna

The array antenna called Antenna 2 is formed by connecting two single rectangular patches with a three-branch feeding network, which follows quarter wavelength transformer approximation, as shown in Fig. 4(a). According to this approximation [15], the first branch of length, L_4 , should have an impedance of 50 ohms, the second branch of length, $2W_2 + W_7$, should have an impedance of 70.71 ohms, and the branches connected to the patches of length L_3 should have an impedance of 100 ohms. The widths of these branches of lengths L_4 , $2W_2 + W_7$, and L_3 are respectively 31 μm , 18 μm , and 9 μm , determined using the CST software's macro function. This array antenna is simulated using the time domain solver in the Frequency range of 0.05 THz to 5 THz. It is found that the antenna causes two frequencies of resonances at 99.4 GHz (84.3 GHz to 113.6 GHz) and 286.5 GHz (274.6 GHz to 298.3 GHz), as depicted in Fig. 4 (b). The first resonance covers the W band of 6G, but the impedance matching is very poor, although the gain is also enhanced. So, further optimization is needed to get a wideband antenna that matches well.

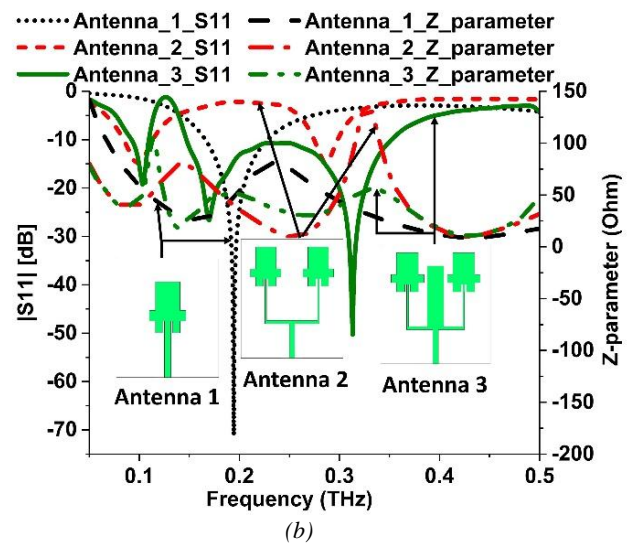
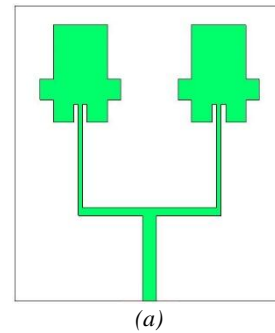


Fig. 4. (a) Patch of Antenna 2 and (b) Comparison of reflection coefficients of Antenna 1, Antenna 2 and Antenna 3 (colour online)

2.2. Design of matching circuit

A rectangular structure of length L_2 and width W_5 is loaded in the middle of the two elements of the array structure and connected at the center of the three-branch feeding network, as depicted in Fig. 5 (a). This configuration can be called Antenna 3, which also shows dual band characteristics. The lengths and widths of this rectangular structure, the size of the ground plane, the dimension of the inset structures, and the positions of the rectangular blocks attached to the patch elements are optimized to make these bands resonate at the desired positions while having a wideband property, good impedance matching, good level of miniaturization and acceptable gain. The optimized matching circuit with the other optimized values of the array elements causes two resonances. The first resonance covers the W band of 6G, ranging from 92.3 GHz to 109.6 GHz, with the resonant frequency recorded at 103.2 GHz. In this band, a good level of miniaturization is achieved where the antenna size is only one-fifth of the operating wavelength in free space at the center frequency. The second resonance is very wide, ranging from 147.1 GHz to 352.1 GHz having a percentage bandwidth of about 82.13 %. This huge bandwidth has two dips, one at 169.7 GHz and the other at 313.1 GHz, with a very good S11 level of -26.65 and -50.1 dB, respectively. Again, the gain achieved after this optimization is the maximum among the three antennas, as shown in Fig.5 (b). As mentioned earlier, several parametric analyses are done on the antenna parameters to optimize the antenna performance.

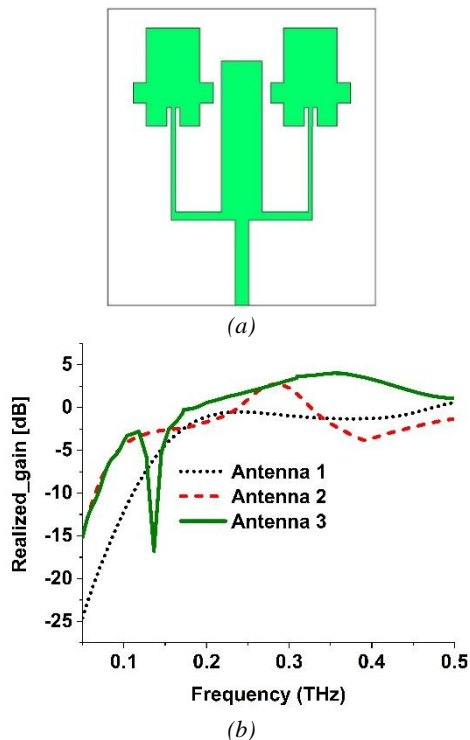


Fig. 5. (a) Patch of Antenna 3 and (b) Comparison of realized gain of Antennas 1, 2 and 3 (colour online)

2.3. Parametric analysis

2.3.1. Matching circuit

First, a parametric analysis is done on the length and width of the matching circuit to see the effect of the reflection coefficient. It is found that increasing the length of the structure decreases the bandwidth of the first band slightly by shifting the upper cut-off frequency to the lower frequency region without changing the position of the resonant frequency. On the other hand, the position of the lower cut-off frequency does not change. But simultaneously increases the bandwidth of the second band, as shown in Fig. 6 (a). More specifically, when the value is increased to $270 \mu\text{m}$, a new dip in the low-frequency region is observed. The optimized value of the length is $330 \mu\text{m}$, which makes the position of the first dip so that it causes the maximum bandwidth and ensures the best $|S_{11}|$ level for both dips.

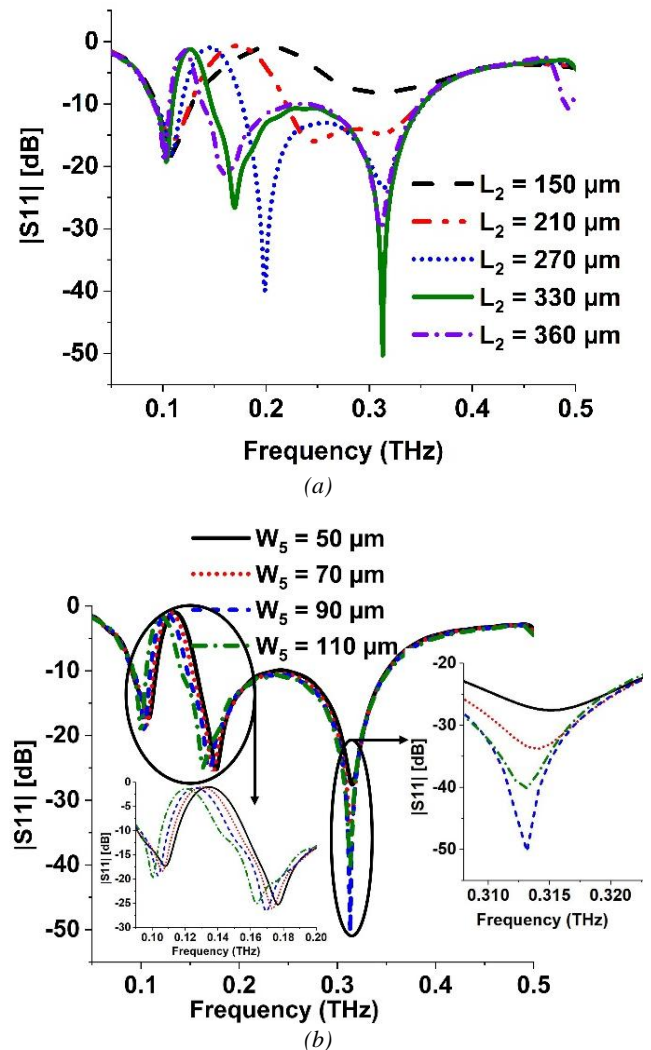


Fig. 6. Parametric analysis of (a) length and (b) width of the matching circuit on the reflection coefficient (colour online)

On the other hand, the parametric analysis of the width reveals that increasing the width shifts the upper cut-off

frequency slightly and the resonant frequency of the first band to the lower frequency region without changing the position of the lower cut-off frequency. Thus, the bandwidth is somewhat reduced, as reported in Fig 6 (b). In this case, a slight improvement in the S11 level is observed. On the other hand, this increment slightly shifts the lower cut-off frequency and the resonant frequency of the second band to the lower frequency region; thus, the bandwidth is increased somewhat. However, a radical change in the S11

level of the second dip is observed. An optimized value of $90\ \mu\text{m}$ will give the best level of S11 for both dips.

2.3.2. Rectangular blocks and inset structures

Other parametric analyses are done on the position of the rectangular blocks and the lengths and widths of the inset structures.

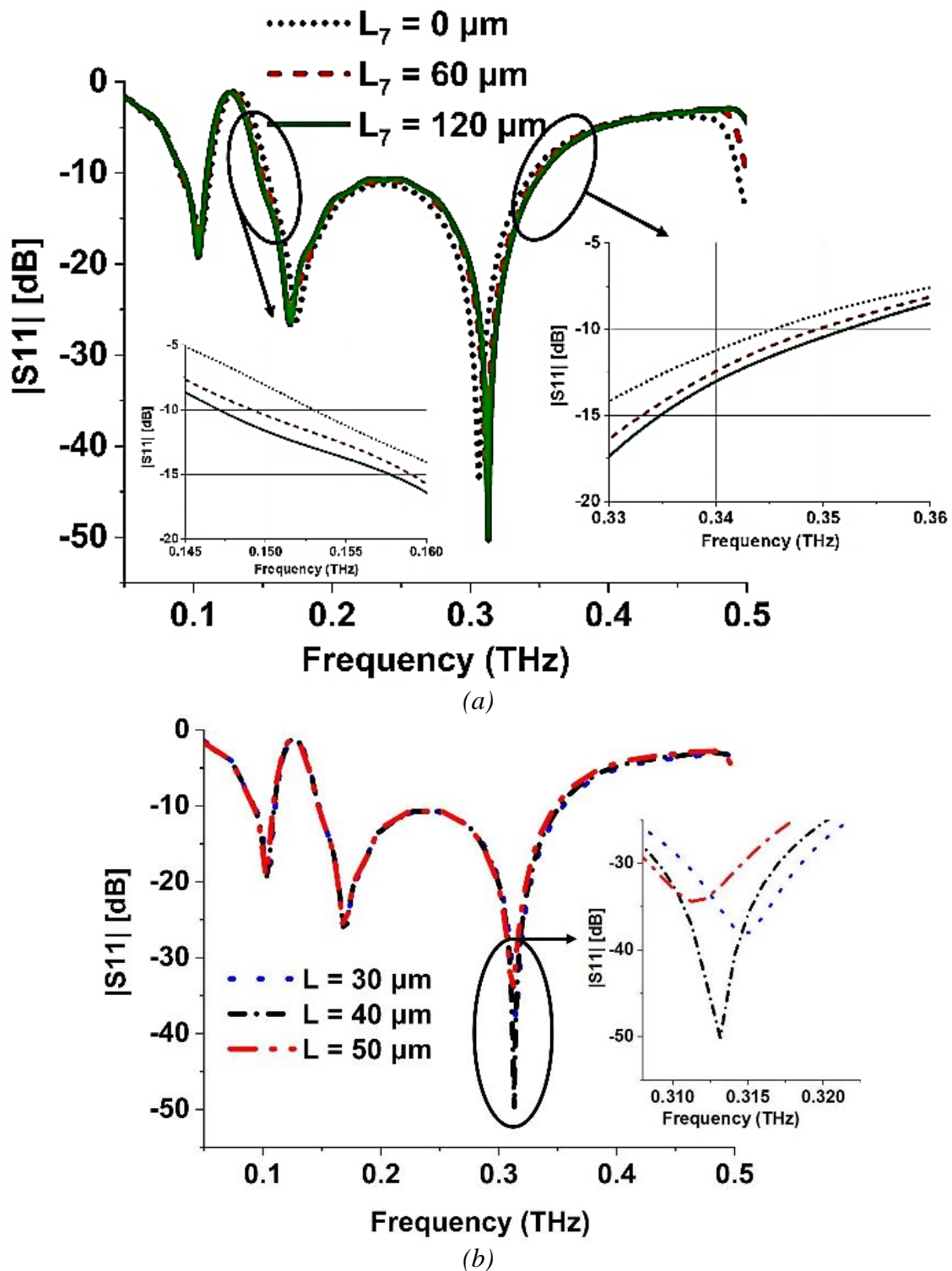


Fig. 7. Parametric analysis of (a) Rectangular block position and (b) Inset length on the reflection coefficient (colour online)

The position of the blocks varies from the edge of the patch to the bottom. As the blocks are moved to the bottom side, the second band's bandwidth increases, as shown in Fig. 7 (a). For instance, by shifting the blocks from the edge to the position where $L_7 = 120 \mu\text{m}$, the lower cut-off frequency moves from 152.99 GHz to 147.1 GHz, and the upper cut-off frequency moves from 345.3 GHz to 352.1 GHz. So, a total increment of almost 13 Hz is achieved. A further increment will degrade the level of S11. The effects of the first band for this position movement are negligible. On the contrary, the length and width variations of the inset structures only affect the S11 level of the second dip of the second band. Only the effect of the length variation is shown in Fig. 7(b). It is observed that an increment of the inset length decreases the level of S11. The optimized value is $40 \mu\text{m}$.

2.4. Current distribution analysis

The current distributions of the bands' resonating points allow for a detailed analysis of how the resonances are generated. Three dips at 103 GHz, 171 GHz, and 313 GHz are observed from these two bands.

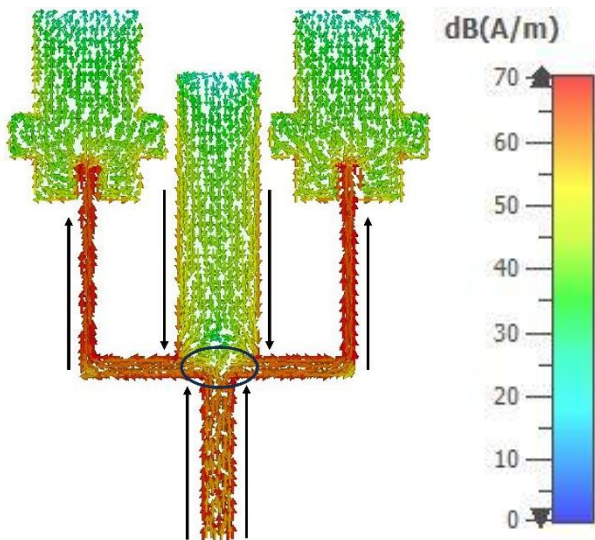


Fig. 8. Current distribution at 103 GHz (colour online)

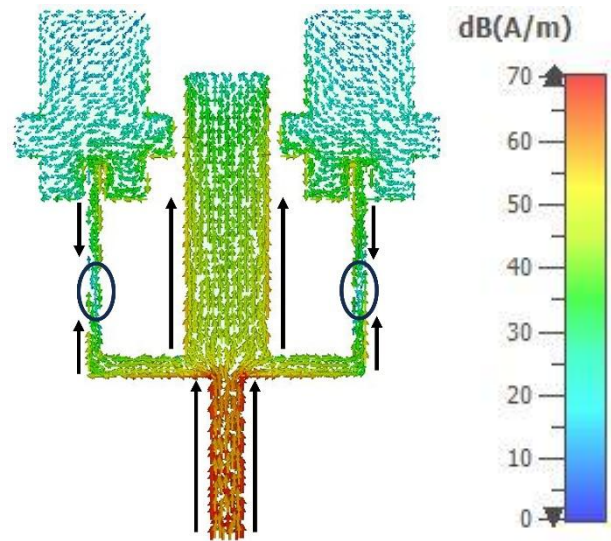


Fig. 9. Current distribution at 171 GHz (colour online)

The current distributions at these dips with the direction indicator lines are given in Fig. 8 and Fig. 9. From the distributions; it is evident that the desired electrical lengths of the corresponding resonances are formed by generating one or more null points at different locations. A null point can be defined as the ending or starting point of one or more current vectors. For the first band, the direction of the current vectors in the branches of the feed line is opposite to the direction of the current vector in the matching circuit. For this reason, only one null point is observed at the joining point of the feeding network with the matching circuit, as shown in Fig. 8. This null point is responsible for the resonance in this band.

On the other hand, as it is well known that current bends at a higher frequency, more null points are found at the current distribution of the dips in the second band. For the first dip of the second band, the current vectors at the first feed line of 50 ohms are in the same direction as the current vector at the matching circuit, as depicted in Fig. 9. So, no null points are found at their junction. But the current vectors at each feedline of 100 ohms are in opposite directions, i.e., one current vector is coming from the patch, and another current vector is flowing from the feed line of 70.71 ohms towards the patch. That's why two null points are found in the two feedlines of 100 ohms. These points are responsible for this dip.

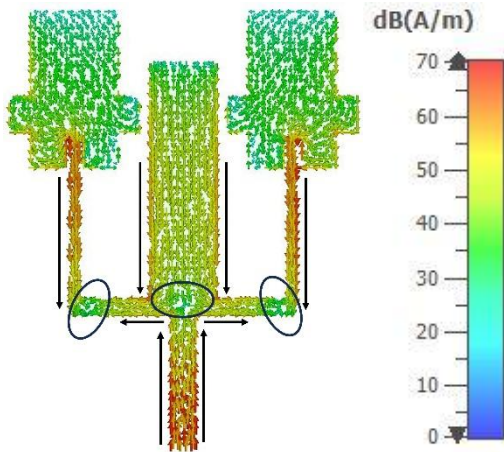


Fig. 10. Current distribution at 313 GHz (colour online)

Finally, for the second dip of the second resonance, the direction of current vectors of the feed line of 50 ohms and the matching circuit follows an opposite direction, which generates a null point at their junction, as presented in Fig. 10. In addition, another two null points are formed in the feed line of 70.71 ohms, which is like the null points of the first dip because in this case the currents flow similarly. But in this case, the positions of the null points are changed. These three null points are responsible for this second dip. From this analysis, it can be said that because of the presence of the matching network, an additional null point is caused, which in turn creates an extra dip in the second band at the high-frequency region. These two dips are then positioned closely so that the bandwidth is maximized.

3. Result analysis

The antenna is simulated using CST microwave studio software with a time domain solver. A waveguide port is used to excite the structure. From the simulation, it is found that the array antenna exhibits dual band characteristics. The reflection coefficient and the realized gain curves are shown in Fig. 11.

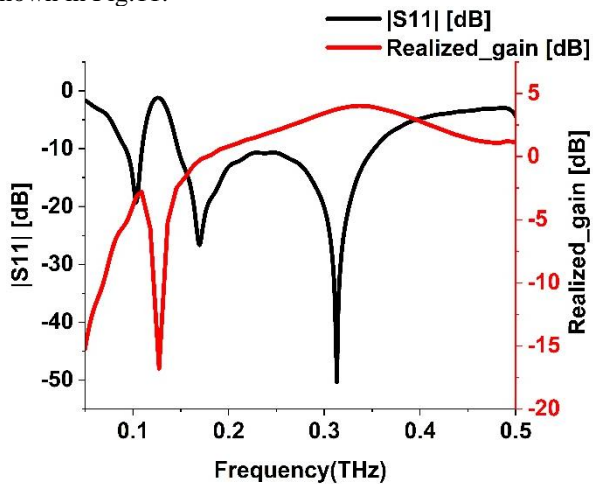


Fig. 11. The reflection coefficient and the realized gain of the proposed array antenna (Antenna 3) (colour online)

The impedance bandwidth of the first band is almost 17.93 %, and the second band is nearly 82.13 % for $|S_{11}| < -10$ dB. The realized gain for the first band varies from -5.3 dBi to -2.95 dBi, where the pick gain is -2.8 dBi. Again, the realized gain for the second band varies from -2.34 dBi to 3.91 dBi, whereas the pick realized gain is 4.03 dBi. Both the gain variations are stable.

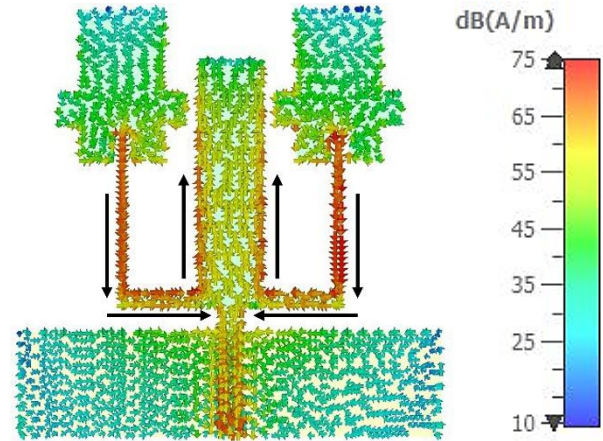


Fig. 12. Simulated surface current distribution at 127.3 GHz (colour online)

The radiation patterns in the E and H planes of the proposed antenna are also investigated, which is shown in Fig. 13 and Fig. 14. It is revealed that the E-plane radiation patterns shown in Fig. 13(a) and Fig. 14(a) for both the resonances are dumbbell shaped. Meanwhile, the H-plane radiation patterns presented in Figs. 13(b) and 14(b) for both resonances are omnidirectional. More concisely, for the first band, the gain variation in the H-plane is very low, only 0.63 dBi. Moreover, the cross-polarization levels in both E and H planes at 103 GHz are very low, less than -46 dBi in the H-plane and -51 dBi in the E-plane. On the other hand, the cross-polarization levels are less than -17 dBi in the H-plane and -54 dBi in the E-plane at 313 GHz. All the radiation patterns are found to be stable. A comparison between the proposed antenna and the other latest research works is listed in Table 2. From the table, it is found that the proposed antenna gives the best compact structure. At the same time, it shows the best wideband solution where several 6G bands of the sub-terahertz region are covered. In terms of bandwidth, the proposed antenna shows the best wideband property. Whereas in terms of realized gain, several research works show higher peak gain than this antenna, for example, the references [3,4], [6,7], and [9], but in terms of compactness and the bandwidth the proposed antenna is superior to them.

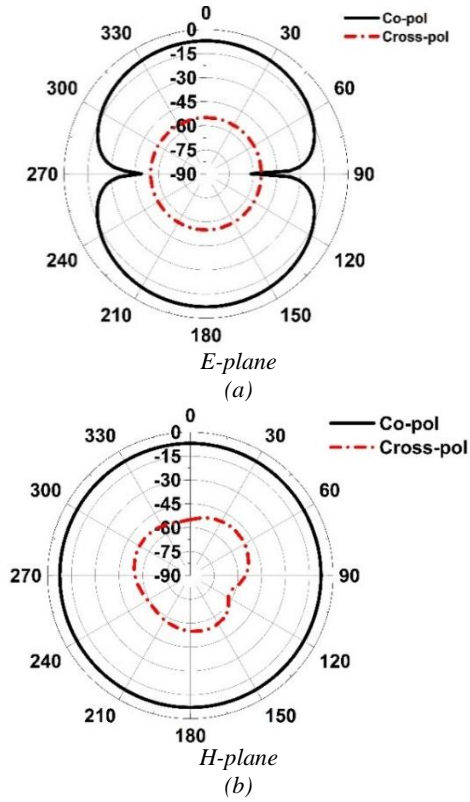


Fig. 13. (a) The E-plane and (b) H-plane radiation pattern of the proposed antenna (Antenna 3) at 103 GHz (colour online)

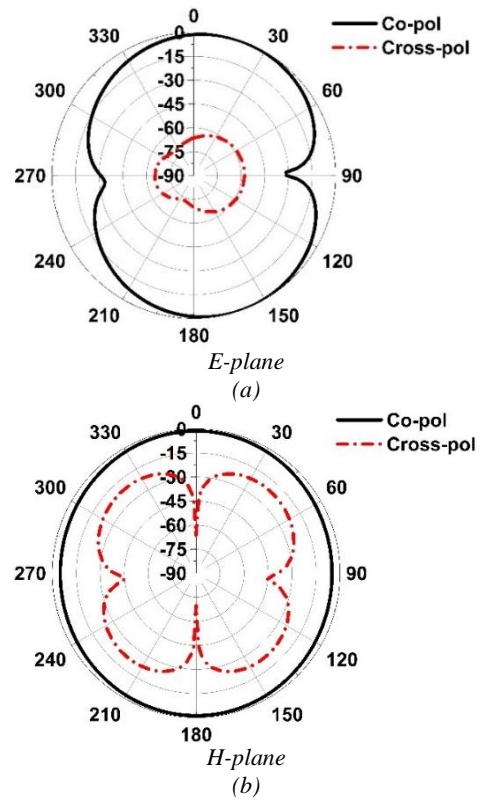


Fig. 14. (a) The E-plane and (b) H-plane radiation pattern of the proposed antenna (Antenna 3) at 313 GHz (colour online)

Table 2. Comparison with Other Recent Research Works with the proposed antenna

Reference	Substrate	Size [$W \mu\text{m} \times L \mu\text{m} \times H \mu\text{m} (\lambda_3)^a$]	-10 dB S ₁₁ BW% (GHz)	Working Band	Gain (dBi)
[7]	polyamide	1500 × 1000 × 150 (0.62 × 0.41 × 0.062)	3.57 (4.4) 8.9 (16)	123 GHz (D band) 180.4 GHz (G band Partially)	4.12 5.05
[8]	PTFE	270 × 310 × 40 (0.89 × 1.02 × 0.13)	45.05 (446)	(767–1213) GHz (Terahertz band)	7.13
[9]	Quartz	1225.71 × 648.88 × 140 (1.67 × 0.88 × 0.192)	34.2 (250)	(285–535) GHz (H band partially and terahertz band)	5.25
[10]	FR4	500 × 500 × 50 (1.35 × 1.35 × 0.135)	11.4, 23 (92, 296)	(761–853) GHz (1.117–1.413) GHz Terahertz band	6.14 7.31
[11]	Rogers RT Duroid 6006	1000 × 1000 × 100 (2.46 × 2.46 × 0.25)	3.2, 2.3, 4.4	725–748.5) GHz (752.5–770) GHz (775–810) GHz Terahertz band	10
[12]	polyamide	300 × 300 × 45 (0.48 × 0.48 × 0.072)	48 (229.1)	(362.7–591.8) GHz Terahertz band	4
[13]		3500 × 3500 × 270 (approx.) (1.28 × 1.28 × 0.098)	35.2 (38.5)	(90–128.5) GHz W band	7.95
[14]	Rogers RT/Duroid 6010	100 × 130 × 45 (0.27 × 0.345 × 0.12)	56.6 (450)	(0.57–1.02) GHz Terahertz band	3.47
Proposed	Rogers RT Duroid 5880	600 × 650 × 10 (0.2 × 0.22 × 0.0034)	17.13 82.13	(92.3–109.6) GHz (147.1–352.1) GHz W, H and G bands	-2.8 4.03

^a Here, λ is the operating wavelength in free space at the center frequency

4. Conclusion

In this paper, a compact and wideband array antenna with a novel matching network is designed. Without the matching network, the array antenna gives dual-band resonance with poor bandwidth and matching. The loading of the matching network causes an additional null point within the second band at a high frequency, which in turn causes additional dips in that band. Important parameters are optimized carefully to place these two dips closely enough to get a maximum bandwidth with the best level of reflection coefficient where the other band remains almost unaffected. The simulated fractional bandwidths are 17.13 % for the first band and 82.13 % for the second band, with the peak gains realized at -2.08 dB and 4.03 dB, respectively. The first band covers the W-band of 6G, the second band covers the entire H-band and partial G band of 6G. The antenna also achieves a great level of miniaturization, which is only one-fifth of the operating wavelength at the center frequency of the first band. Both bands' radiation patterns at the resonance points in the E-plane are dumbbell-shaped.

Meanwhile, the radiation patterns in the H-plane for both bands are omnidirectional. Among them, the first band shows very low gain variation in the H-plane, which is only 0.63 dB. The cross-polarization levels in both planes for both bands are reported to be very low, and the maximum cross-polarization level in the H-plane for the second band is less than -17 dB. The compactness and wideband achieved in this research work are appropriate for the sub-Terahertz applications of 6G.

References

- [1] <https://www.keysight.com/my/en/solutions/emerging-technologies/6g-technology.html>
- [2] <https://www.keysight.com/my/en/assets/3123-1627/white-papers/Exploring-the-6G-Spectrum-Landscape.pdf>
- [3] A. K. M. A. H. Siddique, R. Azim, M. T. Islam, *International Journal of Microwave and Wireless Technologies* **11**(7), 711 (2019).
- [4] R. Azim, M. T. Islam, N. Misran, *Telecommunication Systems* **52**(2), 1171 (2013).
- [5] M. M. Alam, R. Azim, N. M. Sobahi, A. I. Khan, M. T. Islam, *Scientific Reports* **12**(1), 1 (2022).
- [6] M. S. Talukder, M. Samsuzzaman, M. T. Islam, R. Azim, M. Z. Mahmud, M. T. Islam, *Chinese Journal of Physics* **72**, 310 (2021).
- [7] A. Youssef, I. Halkhams, R. El Alami, M. O. Jamil, H. Qjidaa, *Scientific African* **24**, e02196 (2024).
- [8] V. Kumar, A. Chandra, R. Kumar, *Optical and Quantum Electronics* **56**(7), 1176 (2024)
- [9] G. K. Pandey, R. R. Thipparaju, M. K. Rana, *Optical and Quantum Electronics* **56**(6), 1039 (2024).
- [10] K. K. Naik, *Wireless Networks* **30**(4), 2343 (2024).
- [11] A. S. Alqahtani, *Optical and Quantum Electronics* **55**(11), 1014 (2023).
- [12] S. Kiani, P. Rezaei, M. Fakhr, *Journal of Optics* **52**(2), 860 (2023).
- [13] M. H. Maktoomi, Z. Wang, H. Wang, S. Saadat, P. Heydari, H. Aghasi, *IEEE Transactions on Antennas and Propagation* **70**(11), 10047 (2022).
- [14] M. Krishna Ch, T. Islam, N. Suguna, S. Vara Kumari, R. Delshi, Howsalya Devi, S. Das, *Results in Optics* **12**, (2023).
- [15] C. A. Balanis, *Antenna Theory Analysis and Design*, John Wiley & Sons Inc., Hoboken, 866 (2005).

*Corresponding authors: mdmushfiqur@mmu.edu.my;
sujitarpon171@gmail.com;
shabiul.islam@mmu.edu.my